

## Study of Analysis Modeling for Deformation Behavior and Reverse Transformation of Ti-Ni Alloys

Keisuke OKITA\*, Nagatoshi OKABE\*, Tomoyuki SATO\*, Takashi NAKAO\*

\*Ehime University, 3, Bunkyo-cho, Matsuyama, Ehime  
 Fax: 81-089-927-9707, e-mail: verve@zairiki.me.ehime-u.ac.jp

This research aimed to clarify the characteristics of shape memory effect in Ti-Ni SMAs. Considering the appearance mechanism of shape memory effect, both the shape recovery and the recovery force of SMA greatly depend on the state of deformation in the material after pre-deformation. Therefore, it is very important to understand enough the deformation mechanism and its transforming behavior in the loading process, in order to use successfully the shape memory effect. Then, as to clarify the characteristics of shape memory effect, not only the reverse transformation in the heating process but also the deformation mechanism in the pre-deformation process was modeled. And the shape memory effect was made clear though FEM analysis for the model. In addition, the validity of the analysis model was experimentally conducted.

Key words: shape memory effect, FEM analysis, Schmidt factor, mixed deformation

### 1. INTRODUCTION

Shape memory alloy has a great characteristic of recovering to the original shape by heating, even if it is subjected to a large deformation in martensitic state. This characteristic is called the shape memory effect, and the alloys are used for various applications such as coupling devices and actuators in electric appliance, etc [1].

The mechanism of shape memory effect can be explained as follows. By martensitic transformation, the alloys form the martensite variants with various different orientations from the same parent phase. The martensite variants can be easily reoriented by external stress to be quite mobile. If the temperature is raised, the reverse transformation occurs, and the oriented martensite variants revert to the parent phase in the original orientation [1]. Thus, the amounts of the recovery strain and recovery stress are determined by the strain of oriented martensite variants. Therefore, in order to use the shape memory effect appropriately, it is important to understand enough the deformation mechanism in the martensitic state of the alloy. However, the deformation mechanism of martensite variants is more complex in a polycrystal [2]. Since the sensibilities to external stress in each crystal grain are respectively different due to the difference of Schmidt factor, the deformation by reorientation of martensite variants develops with not only elastic deformation but also slip deformation [3].

Then, in this paper, the authors suggest a new deformation model in which Schmidt factor was considered. Deformation behavior of the alloy in martensitic state was simulated with FEM analysis, and the recovery strains that depend in large measure on pre-deformation were predicted. In addition, the results of the analysis model were verified by experiments.

### 2. ANALYSIS MODEL

#### 2-1 Modeling for deformation

Figure 1 shows the typical stress-strain curve of uniaxial tensile test in the martensitic state. The deformation behavior has been explained as follows.

The stress-strain curve consists of four stages ("I" to "IV") corresponding to the strain range, respectively. Stress-strain curve in the stage "I" obeys the elastic deformation of martensite variants until reaching the stage "II". The reorientation of martensite variants proceeds in the stage "II", and it completes at the end of the stage "II". In the stage "III", the reoriented martensite variants deform elastically with a rapidly increasing stress. A second apparent yield occurs with further applied strain (the onset of the stage "IV"). The deformation proceeds in a typical manner of slipping influenced by strain hardening. However, this interpreta-

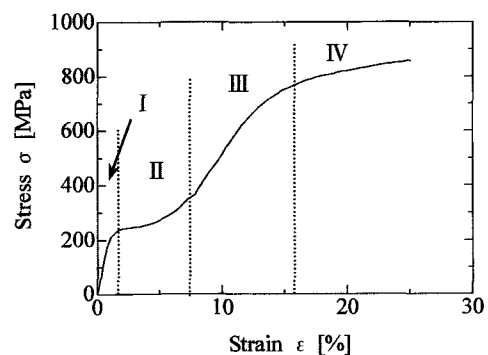


Fig. 1: Typical deformation behavior of martensite.

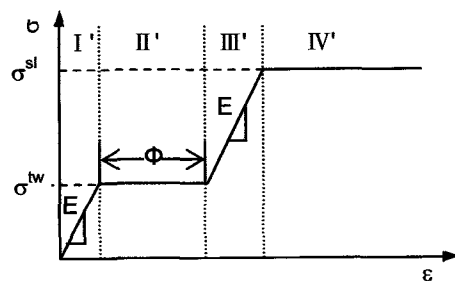


Fig. 2: Deformation behavior of any element in modeling.

tion disagrees with results of our experiment as well as previous study in several aspects [3-5]. The following facts have already been clarified experimentally. The deformation by slipping as well as reorientation was generated even in the stages "I" and "II". Moreover, in the stage "III", the reorientation of martensite variants also continues to proceed following the stage "II". These phenomena suggest that the deformation in martensite is composed of elasticity deformation, reorientation of martensite variants and slipping deformation. We consider that the mixed deformation is likely associated with Schmidt factor in the polycrystal. That is, the uniaxial tensile stress changes in magnitude depending on the crystal orientations on the basis of Schmidt factor, and as a result, some manners of deformation are mixed in a polycrystal.

Now, let's explain the modeling of such a mixed deformation in martensitic state of our proposal.

In modeling for the deformation, stress-strain curve of individual element was modeled as the simple deformation behavior as shown in Fig. 2. The strain regions ("I'"-"IV'") in the figure correspond to the manners of deformation in stages ("I"-"IV") in Fig. 1, respectively. However, in each region, the mixed deformation doesn't occur, but only one manner of deformation occurs. And, two yield stresses  $\sigma^{tw}$  and  $\sigma^{sl}$  (the former is a critical stress for generating the reorientation of martensite variants, the latter is a critical stress for slipping the reoriented martensite.) vary with the element. A polycrystalline matrix was modeled as an aggregate of such elements, and consequently the stress-strain curve exhibits the mixed deformation behavior with some manners of deformation. In addition, the plastic deformation with both the reorientation of martensite variants in the region "II'" and the slip in the region "IV'" is assumed not to occur work-hardening, and so the stress-strain curve is modeled as elastic-perfectly plastic body with two levels of yield stress as shown in Fig. 2. Every element is assumed to have the same Young's modulus  $E$  in the both region of "I'" and "III'". Both yield points of  $\sigma^{tw}$  and  $\sigma^{sl}$  are assumed to obey the extreme value distribution function of equation (1) and (2), respectively. Then, since the strain due to martensite reorientation  $\Phi$  in each element can be supposed to be the complementary event of  $\sigma^{tw}$ , the  $\Phi$  is determined by equation (3).

$$F^{tw}(\sigma^{tw}) = 1 - \exp\left\{-\left(\frac{\sigma^{tw}}{\tilde{\sigma}^{tw}}\right)^{\alpha_{tw}}\right\} \quad (1)$$

$$(0 \leq \sigma^{tw} < \infty, \alpha_{tw} > 0, \tilde{\sigma}^{tw} > 0)$$

$$F^{sl}(\sigma^{sl}) = 1 - \exp\left\{-\left(\frac{\sigma^{sl}}{\tilde{\sigma}^{sl}}\right)^{\alpha_{sl}}\right\} \quad (2)$$

$$(0 \leq \sigma^{sl} < \infty, \alpha_{sl} > 0, \tilde{\sigma}^{sl} > 0)$$

$$F^{\Phi}(\varepsilon^p) = \exp\left[-\left\{\frac{(\Phi_{\max} - \varepsilon^p)^{\alpha_{\Phi}}}{(\Phi_{\max} - \tilde{\Phi})}\right\}\right] \quad (3)$$

$$(0 \leq \varepsilon^p \leq \Phi_{\max} < \infty, \alpha_{\Phi} > 0, 0 < \tilde{\Phi} < \Phi_{\max})$$

Where,  $\tilde{\sigma}^{tw}$ ,  $\tilde{\sigma}^{sl}$  and  $\tilde{\Phi}$  are scale parameters, and  $\alpha_{tw}$ ,  $\alpha_{sl}$ , and  $\alpha_{\Phi}$  are shape parameters.  $\Phi_{\max}$  is the maximum value of the strain due to martensite reorientation in the distribution of the  $\Phi$ . And  $\varepsilon^p$  denotes the equivalent plastic strain that adds the strain due to martensite reorientation to the strain due to slip. The  $\tilde{\sigma}^{tw}$ ,  $\tilde{\sigma}^{sl}$  and  $\tilde{\Phi}$  were determined by experimental data. On the other hand the  $\alpha_{tw}$ ,  $\alpha_{sl}$  and  $\alpha_{\Phi}$  were determined by changing their values so that stress-strain curve can fit well to the experimental data, namely by the way of the inverse analysis.

## 2-2 Modeling for reverse transformation after pre-deformation

Figure 3 shows a schematic representation exhibiting the recoverable strain due to reverse transformation by heating with the deformation in martensitic state [6]. The regions ("I'"-"IV'") in the figure correspond to those of Fig. 2. Since the deformation due to slip never occurs in the regions of "II'" and "III'", the equivalent plastic strain  $\varepsilon^p$  is equal to the strain due to martensite reorientation  $\varepsilon^{tw}$  in these regions. Namely, the recoverable strain due to reverse transformation  $\varepsilon^r$  becomes to be equal to the  $\varepsilon^{tw}$ . In such case as the martensite variants orient completely in one direction on completing the martensite reorientation, the recoverable strain  $\varepsilon^r$  equals to  $\Phi$  and is the maximum. By further deformation, the strain due to slip  $\varepsilon^{sl}$  starts to occur in the region "IV'" as shown in Fig. 3. Since the  $\varepsilon^{sl}$  is not recoverable even if heated, the  $\varepsilon^{sl}$  remains in the material as permanent strain. And, the equivalent plastic strain  $\varepsilon^p$  in this region "IV'" can be expressed by  $(\Phi + \varepsilon^{sl})$ , and so the recoverable strain  $\varepsilon^r$  is  $\Phi$  also. In the region "IV'", the strain due to slip  $\varepsilon^{sl}$  increases with increasing of the deformation. Therefore, the permanent strain after heated increases with increasing of the  $\varepsilon^{sl}$ , but the recoverable strain  $\varepsilon^r$  is still  $\Phi$ .

Where, equivalent plastic strain  $\varepsilon^p$  is defined by equation (4) based on total strain theory.

$$\varepsilon^p = \sqrt{\frac{2}{9} \left\{ (\varepsilon_x^p - \varepsilon_y^p)^2 + (\varepsilon_y^p - \varepsilon_z^p)^2 + (\varepsilon_z^p - \varepsilon_x^p)^2 + \frac{3}{2} (\gamma_{xy}^p{}^2 + \gamma_{yz}^p{}^2 + \gamma_{zx}^p{}^2) \right\}} \quad (4)$$

And, each components of recovery strain  $\varepsilon_i^r$  are determined as follows.

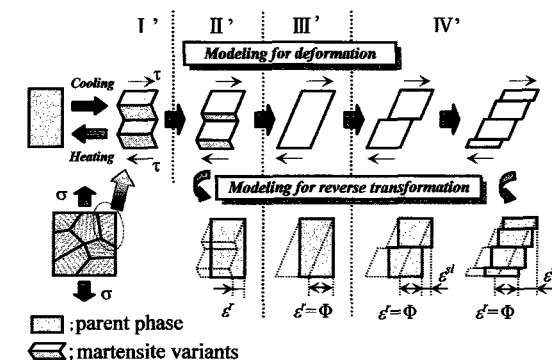


Fig. 3: Model chart concerning the deformation mechanism and the reverse transformation.

In the regions “II'” and “III'”, in other words, in  $\varepsilon^p \leq \Phi$ , the recovery strain is given as follows;

$$\varepsilon_{ij}^r = \varepsilon_{ij}^p \quad (5)$$

On the other hand, in the region “IV'” ( $\varepsilon^p > \Phi$ ), the recovery strain is given as the strain  $\varepsilon^{rP}$  at momentary point that the condition of  $\varepsilon^p > \Phi$  is satisfied.

$$\varepsilon_{ij}^r = \varepsilon_{ij}^{rP} \quad (6)$$

And so, the recovery strain  $\varepsilon_{ij}^r$  is modeled as thermal strain  $\varepsilon_{ij}^h$ , which is used as the following equation (7) in the FEM analysis.

$$\varepsilon_{ij}^h = \sum \left( -\frac{\varepsilon_{ij}^r}{T_f^A - T_s^A} \cdot \Delta T \right) \quad (7)$$

Where,  $T_s^A$  indicates the starting temperature of reverse transformation,  $T_f^A$  the finishing temperature, respectively. Namely, The  $\varepsilon_{ij}^r / (T_f^A - T_s^A)$  implies to be a coefficient for calculating the apparent thermal reduction strain due to reverse transformation. The  $\Delta T$  is an incremental temperature per a step in the FEM analysis.

### 3. ANALYSIS METHOD

In this analysis, for reasons of symmetry, only one-quarter of the SMA wire specimen is used to be modeled. 2808 elements are used for the mesh with 10 elements for the radius direction and 24 elements for axis direction. The geometry of the wire and a mesh are shown in Fig. 4. The boundary conditions are given as displacement-free along the line of  $r=0$  and  $z=0$  due to symmetry. Also, constraint displacement is given along axis direction for loading and unloading of tension.

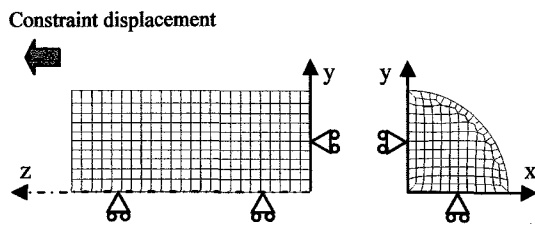


Fig. 4: Finite element mesh.

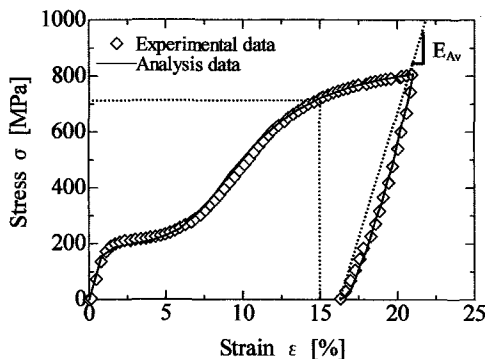


Fig. 5: stress-strain curve fitted well to experimental data.

## 4. EXPERIMENT

### 4-1 Specimens

Ti-Ni-Nb shape memory alloys were hot forged and hot extruded, and followed by cold drawing and intermediate annealing to make wires with a diameter of 1.0mm. The alloys are composed of Ti-45.5Ni-9Nb [at%]. The wires were finished by cold drawing with CW=30% reduction and were cut to 95.0mm in length. The specimens were solution treated at  $T_{ST}=1223K$  for 3.6ks, and followed by water quenched. Specimens were cooled in liquid nitrogen prior to experiments to ensure to a martensite structure. In addition, transformation temperatures were determined from the DSC measurement to be  $M_s=278K$ ,  $M_f=282K$ ,  $A_s=318K$  and  $A_f=329K$ .

### 4-2 Experimental procedure

In the experiment, the thermo-mechanical history was applied to each specimen as follows; ①The specimens were deformed up to various levels of maximum applied strain  $\varepsilon_{max}$  at room temperature, which was about 20K below the  $A_s$  temperature of the specimen. ②They were unloaded at the same temperature. ③They were heated until the reverse transformation had finished under free stress. For every levels of maximum applied strain  $\varepsilon_{max}$  the deformation behavior in loading / unloading process were measured, and followed by measuring the recovery strain  $\varepsilon^r$  due to heating.

## 5. RESULT AND DISCUSSION

### 5-1 Stresses-strain behavior

Figure 5 shows the analytical stress-strain curve which was fitted well for the experimental stress-strain

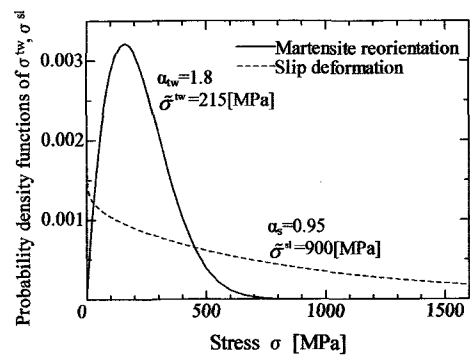


Fig. 6: Probability density functions of  $\sigma^{tw}$  and  $\sigma^{sl}$  obtained by inverse analysis.

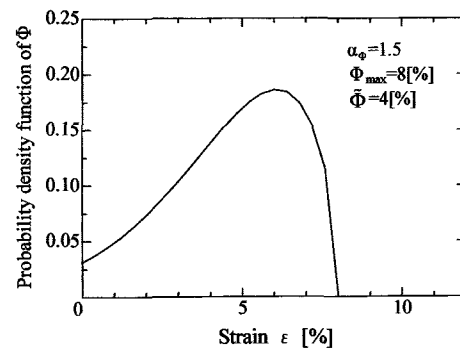


Fig. 7: Probability density functions of  $\Phi$  obtained by inverse analysis.

curve to determine the parameters in the equations (1) to (3). The analytical stress-strain curve can estimate well both behaviors of the mixed deformation in loading and the nonlinear deformation in unloading. Figure 6 shows the probability density functions of the extreme value distribution function (1) to (3) determined by this inverse analysis method. The shape parameter for the case of deformation due to slip  $\alpha_s$  is below 1 and so the distribution of  $\sigma^s$  indicates an exponential distribution as shown in figure. Thus, the deformation due to slip is suggested to occur in even early stage of deformation such as the stages "I" and "II". This result is well consistent with previous study.

### 5-2 Dependency of characteristics on applied strain

The parameters determined by the inverse analysis method can apply to predict the dependencies of characteristics on pre-deformation, which was estimated quantitatively using the maximum applied strain  $\varepsilon_{\max}$ .

Figure 8 shows the comparison of the analytical prediction with the experimental data in order to evaluate the prediction for the dependency of average elasticity modulus  $E_{AV}$  in unloading process. The analysis result for the  $E_{AV}$  corresponds with the experimental behaviors for the  $E_{AV}$  decreasing with increasing of  $\varepsilon_{\max}$ . The decreasing mechanism for the  $E_{AV}$  can be explained from this analysis result as described below.

Even on applying the bulk total pre-strain  $\varepsilon_{\max}$  with a certain uniform magnitude, the total pre-strain magnitude of every element varies with the each stress level of  $\sigma^w$  and  $\sigma^sl$  given in the analysis. Therefore, the elastic recovery strains in whole unloading are different individually in every element. The stress levels at unloading starting time, also, are different individually.

The cumulative internal stress due to the strain differences on interfaces between neighbor elements causes the nonlinear deformation behavior in unloading process as shown in Fig. 5. Since the elastic recovery strain is clarified from our previous experiments [5] to increase with increasing of the  $\varepsilon_{\max}$ , the  $E_{AV}$  can be predicted to decrease with increasing of the  $\varepsilon_{\max}$  as shown in Fig. 8.

Figure 9 shows the changing behavior of recovery strain  $\varepsilon^r$  due to reverse transformation with increasing of  $\varepsilon_{\max}$ , compared the analytical prediction with the experimental data. The  $\varepsilon^r$  increases with increasing of  $\varepsilon_{\max}$  within the strain range of 15%, that is, this tendency suggests that martensite reorientation will continue to proceed up to 15% in the applied strain. And, the  $\varepsilon^r$

indicates the maximum value at  $\varepsilon_{\max} \approx 15\%$  in both results of analysis and experiment. From Fig. 5, the applied strain of 15% was seen to correspond to the stress of 700MPa. As shown in Fig. 6 the stress of 700MPa corresponds almost to the maximum value in the distribution of  $\sigma^w$ . In fact, when the stress level reaches to 700MPa, whole elements in the material have finished reorienting completely and the  $\varepsilon^r$  becomes the maximum at the same time. From these facts, it was verified that our proposal model for both the deformation and the reverse transformation can express accurately an actual phenomenon by some equations.

On the other hand, in the range of  $\varepsilon_{\max} > 15\%$  corresponding to the stage "IV", the  $\varepsilon^r$  decreases slightly with increasing of  $\varepsilon_{\max}$ . The dislocation introduced excessively by deformation of slip seems to influence largely the above tendency judging from the experimental fact that the  $\varepsilon^r$  comes to decrease with increasing of the  $\varepsilon_{\max}$ , because it can be assumed enough that the excessive crossed dislocations prevent the shape recovery due to reverse transformation from proceeding.

## 6. CONCLUSION

The modeling for the deformation in martensite state as well as the reverse transformation was conducted in order to clarify the characteristics of shape memory effect. The dependency of the applied strain on the recovery strain  $\varepsilon^r$  was predicted through FEM analysis, based on some model equations obtained by the method of the inverse analysis from the experimental results. The comparison between the results of experiment and inverse analysis could verify our proposal model to be applicable for predicting the behavior of deformation as well as shape recovery.

## REFERENCE

- [1] K. Otsuka and C. M. Wayman: Shape Memory Materials, (Cambridge University press), 1998, 1-41
- [2] Z. Xie, Y. Liu and J. V. Humbeeck, Acta metall., 1998, 46, 1989.
- [3] Y. Liu, Y. Liu and J. V. Humbeeck, Acta mater., 1999, 47, 199.
- [4] S. Miyazaki, K. Otsuka, and Y. Suzuki, Scripta metall., 1981, 15, 287.
- [5] K. Okita, N. Okabe, T. Sakuma, H. Semba and Y. Mihara, Mater. Sci. Forum, 2005, 475-479, 1953.
- [6] Y. Liu, Z. Xie, and J. V. Humbeeck and L. Delaey, Mater. Sci. and Eng., 1999, A273-275, 679.

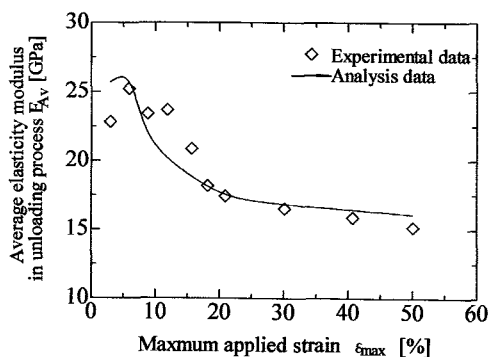


Fig. 8: Comparison between predictions by the simulations and experimental data for  $E_{AV}$  with  $\varepsilon_{\max}$ .

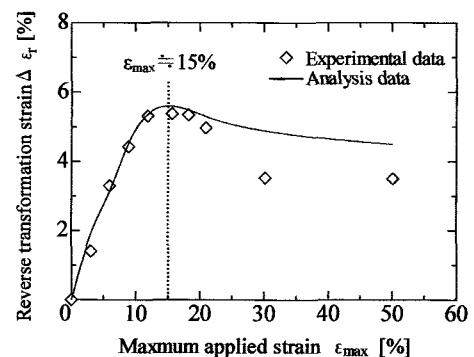


Fig. 9: Comparison between predictions by the simulations and experimental data for  $\Delta\varepsilon_r$  with  $\varepsilon_{\max}$ .